

Efficient computation of free energy of crystal phases due to external potentials by error-biased Bennett acceptance ratio method

Pankaj A. Apte

Department of Chemical Engineering,

Indian Institute of Technology Kanpur, Kanpur, U.P, India 208016

(Dated: November 20, 2018)

Abstract

Free energy of crystal phases is commonly evaluated by thermodynamic integration (TDI) along a reversible path that involves an external potential. A persistent problem in this method is that a significant hysteresis is observed due to differences in the center of mass position of the crystal phase in the presence and absence of the external potential. To alleviate this hysteresis, a constraint on the translational degrees of freedom of the crystal phase is imposed along the path and subsequently a correction term is added to the free energy to account for such a constraint. In this work, we propose a new methodology termed as error-biased Bennett Acceptance ratio (EBAR) method that effectively solves this problem without the need to impose any constraint. This method is simple to implement and it does not require any modification to the path. We show the applicability of this method in the computation of crystal-melt interfacial energy by cleaving wall method [J. Chem. Phys., **118**, 7651 (2003)] and bulk crystal-melt free energy difference by constrained fluid λ -integration method [J. Chem. Phys., **120**, 2122 (2004)] for a model potential of silicon.

I. INTRODUCTION

Accurate evaluation of free energy of a crystal phase by simulation is important to predict many important thermodynamic properties including the melting temperature,¹ the relative stability of different crystal phases² (i.e., polymorphism), and the interfacial free energy of crystal phases.^{3,4} A common method of free energy evaluation is thermodynamic integration (TDI), in which an external potential is imposed on the crystal phase to ensure thermodynamic reversibility,¹ and the method requires that the resulting free energy change be computed accurately. However, the external potential causes center of mass (CM) position of the crystal phase to change relative to that in the absence of the external potential and this leads to hysteresis in the free energy computation. This problem has been reported to occur in many TDI methods including Einstein crystal method,^{1,5} constrained fluid λ -integration method,^{6,7} surface free energy calculation of crystal phases,⁴ and direct computation of crystal-melt interfacial energy by cleaving wall method.³

A variety of constraints are imposed on the translational degrees of freedom of the crystal phase to address this problem. In Einstein crystal method, CM is fixed during thermodynamic integration along the path.¹ In direct computation of crystal-melt free energy difference, CM is either fixed⁶ or confined to a small region.⁷ A fixed particle constraint was also proposed for this method.⁷ In surface free energy calculation of Au[110] crystal phase,⁴ CM velocity was artificially controlled by the (otherwise) dormant external potential during Molecular Dynamics (MD) simulation. In the computation of crystal-melt interfacial energy γ , two crystal layers were immobilized by assigning them an infinite mass throughout the four stage integration path.³ It can be seen from the above examples that although cause of the hysteresis is the same, every TDI path requires its own ad-hoc procedure to constrain the translational degrees of freedom of the crystal phase. Further, the use of a constraint entails computation of the correction term to obtain free energy difference between the unconstrained phases. In case of Einstein crystal method,¹ the correction term can be computed analytically and the effort required is minimal. When CM is confined to a small region in constrained fluid λ -integration method, the correction term needs to be computed by separate simulations.⁷ In cleaving wall method,³ γ was computed for two different system sizes in order to determine the effect of the constraint. Thus, the estimation of the correction term is, in itself, computationally expensive in many cases.

In this article, we propose a new methodology termed as error-biased Bennett acceptance ratio (EBAR) method (to be explained in sec. II) to efficiently compute the free energy change resulting from imposition of the external potential on the crystal phase, *without* requiring the use of any constraint. We demonstrate two applications of this methodology in sec. III. We first compute the free energy of the crystal phase due to repulsive wall potential in cleaving wall method.^{3,8} Next, we compute the free energy difference resulting from the imposition of an attractive Gaussian well potential on the crystal phase in constrained fluid λ -integration method.^{6,7} Both calculations are performed for the Stillinger and Weber⁹ potential of silicon. Finally, we summarize our results and discuss further possible applications of this methodology in sec. IV.

II. ERROR-BIASED BENNETT ACCEPTANCE RATIO METHOD

In this section, we first describe the Bennett acceptance ratio method¹⁰ (BAR) which is routinely employed to compute the free energy difference between two states.^{11,12,13} We then describe the error biased Bennett acceptance ratio (EBAR) method in the context of the present problem. According to the BAR method,¹⁰ Helmholtz free energy difference $\Delta F = F_1 - F_0$ between two equilibrium states ‘0’ and ‘1’ is given by the following equation:¹⁰

$$\Delta F = \log \frac{\sum_1 f(\phi_0 - \phi_1 + C)}{\sum_0 f(\phi_1 - \phi_0 - C)} + C - \log \frac{n_1}{n_0}, \quad (1)$$

where C is a constant, $f(x) = 1/(1 + e^x)$ is the fermi function, \sum_0 and \sum_1 represent the sums over fermi functions sampled in ‘0’ and ‘1’ ensembles, respectively. The symbols ϕ_0 and ϕ_1 in Eq. (1) represent the total configurational energies and n_0 and n_1 are the number of sampled fermi functions in the above two ensembles. Please note that we have expressed ΔF , ϕ_0 , ϕ_1 , and C in units of $k_B T$ and we will follow this convention throughout unless otherwise stated explicitly. The error (in units of $k_B T$) in the free energy estimate is given by $\sigma^2 = \langle (\Delta F - \Delta A)^2 \rangle$, where ΔA is the expectation (correct) value of the free energy difference. When we are in the large sample regime (i.e., both \sum_0 and \sum_1 are reasonably accurate), the variance can be approximated as¹⁰

$$\sigma^2 \approx \frac{\langle f^2 \rangle_0 - \langle f \rangle_0^2}{n_0 \langle f \rangle_0^2} + \frac{\langle f^2 \rangle_1 - \langle f \rangle_1^2}{n_1 \langle f \rangle_1^2}. \quad (2)$$

where $\langle f \rangle_0$ is the ensemble average of $f(\phi_1 - \phi_0 - C)$ evaluated in ensemble 0 and $\langle f \rangle_1$ is the ensemble average of $f(\phi_0 - \phi_1 + C)$ evaluated in ensemble 1. Bennett showed that the

value of $C = C_B$ which minimizes σ^2 is given by the following expression¹⁰

$$\Delta F = C_B - \log \frac{n_1}{n_0}. \quad (3)$$

This value of C corresponds to the condition¹⁰ that $\partial\sigma^2/\partial C = 0$. Thus, in the BAR method, the optimum estimate of ΔF is obtained by solving Eqs. (1) and (3) simultaneously. The condition given by Eq. (3) can also be expressed as $\sum_0 = \sum_1$. The important requirement for the applicability of the BAR method is that the large sample regime should be achieved in both the ensembles.

Considering the present problem, let's denote the crystal phase with and without an external potential as state 1 and 0, respectively. In such a case, the instantaneous configurational energies in the two states are given by $\phi_0=U$ and $\phi_1=U + U_{ext}$, where U is the potential energy due to interactions between the particles and U_{ext} is the external potential energy. Because of the influence of U_{ext} , average position of center of mass of the crystal phase will be different in the two states. In order to sample the perturbation energy $\phi_0 - \phi_1$ efficiently in state 1 the following two conditions are necessary. (i) The important configurations must overlap to a large extent with those of state 0, which is possible if the external potential does not affect the crystal structure significantly. (ii) Further, the external potential must be sufficiently strong so that the CM is localized at the average position \mathbf{R}_1 . If this latter condition is not satisfied, the number of important configurations (corresponding to all possible CM positions) becomes too large and cannot be sampled in a finite length simulation. In state 0, the important values of the perturbation energy $\phi_1 - \phi_0$ are those for which the CM position is \mathbf{R}_1 (corresponding to the state 1) and are therefore not likely to be sampled in a simulation of reasonable length because the CM position can fluctuate wildly in state 0 due to the absence of the external potential. This leads to a large error in the estimate of \sum_0 in Eq. (1) for a given value of C and n_0 .

When conditions (i) and (ii) are satisfied, the value of \sum_1 in Eq. (1) can be estimated accurately in a simulation of reasonable length. However, due to poor estimate of \sum_0 , the large sample regime is not achieved at $C = C_B$ and the BAR method fails. To circumvent this difficulty, we propose the EBAR method, in which we choose an appropriate value of $C = C_E$ (away from C_B) such that the estimate of both \sum_0 and \sum_1 are reasonably accurate and hence the large sample regime is achieved. For this purpose, it is important to note the following two points:

(a) When the value of C is chosen such that $\sum_0 \geq 1$, $\log \sum_0 \approx \log \langle \sum_0 \rangle$,¹⁰ where $\langle \sum_0 \rangle$ is the expectation (accurate) value of \sum_0 at a given C and n_0 (see Fig. 4 of Ref. 10 and the accompanying discussion). In such a case, the main source of error will be due to \sum_1 , which we expect to be sufficiently accurate when the conditions (i) and (ii) given above are satisfied.

(b) In order to locate the exact value of C where a large sample regime will occur, we first consider two limiting cases. When C approaches $C_{+\infty}$, such that $x = (\phi_0 - \phi_1 + C) \rightarrow +\infty$, $f(x) \approx e^{-x}$ and $f(-x) \approx 1$. In this case, Eq. (1) reduces to the single stage free energy perturbation (FEP) formula $\Delta F = \log \langle \exp[-(\phi_0 - \phi_1)] \rangle_1$, where $\langle \cdot \cdot \cdot \rangle_1$ is the NVT ensemble average in state 1. In this limit $\partial \sigma^2 / \partial C = 0$, however, we shall be necessarily in the small sample regime since we are not using any data from the state 0 in the estimation of ΔF [the FEP formula in state 1 can be considered as a limiting case¹⁰ of the acceptance ratio formula in Eq. (1) as $n_0 \rightarrow 0$]. Also at $C = C_B$, $\partial \sigma^2 / \partial C = 0$ according to the BAR method, but the result corresponds to the small sample regime due to the poor estimate of \sum_0 , as discussed before. For an intermediate value of $C = C_E$ ($C_B < C_E < C_{+\infty}$), the magnitude of $\partial \sigma^2 / \partial C$ must attend a local maximum. The large sample regime will occur in the immediate vicinity of C_E , since as we move away from C_E in either direction ($C \rightarrow C_B$ or $C \rightarrow C_{+\infty}$), the magnitude of $\partial \sigma^2 / \partial C$ decreases to 0 and we approach the small sample regime.

To summarize the EBAR method, we choose $C = C_E$ such that the magnitude of $|\partial \sigma^2 / \partial C|$ is at its maximum and $\sum_0 \geq 1$. It may be noted that a local maximum of $|\partial \sigma^2 / \partial C|$ will also exist when $\sum_1 \geq 1$, but it will not correspond to the large sample regime due to poor estimate of \sum_0 . In order that the EBAR method be successful, the estimation of \sum_1 must be sufficiently accurate. This is ensured by the conditions (i) and (ii) mentioned above. As in Ref. 10, the above methodology can be extended straightforwardly to isothermal isobaric (NPT) ensemble. In this case, the values of the perturbation energies in above equations will be sampled during NPT simulations and Eqs. (1)–(3) yield the Gibbs free energy difference ΔG between states 0 and 1 instead of the Hemholtz free energy difference ΔF .

III. APPLICATIONS

In what follows, we demonstrate two applications of the EBAR method for the Stillinger-Weber (SW) potential⁹ of silicon at the previously reported melting point, i.e., at $T^* = 0.0667$ (1678 K) and $P^* = 0^{14}$ (quantities with the superscript * are dimensionless).

A. Cleaving wall method

In cleaving wall method, bulk crystal and melt phases are combined reversibly to form an interface and the work required for this change per unit interfacial area yields the crystal-melt interfacial energy γ .³ This technique is sufficiently precise so as to resolve the anisotropy of γ and has been applied to study anisotropy of interfacial energies of hard-spheres,¹⁵ soft-sphere potential,¹⁶ and to model potentials of silicon⁸ and water.¹⁷ In the first stage of this process, crystal phase is cleaved at a predetermined plane so that no particle can cross that plane. The cleaving is done by introducing a repulsive wall consisting of one or more ideal crystal layers. These layers are chosen to have the same orientation as that of the interface being studied. This process is prone to hysteresis due to center of mass motion of the crystal phase since it changes the relative distance between the wall and the crystal layers. To prevent the hysteresis, Davidchack and Laird³ immobilized particles in the two layers of the crystal phase sufficiently far from the cleaving plane while applying the cleaving potential. To study the effect of this fixed layer constraint, thermodynamic integration was performed with the same interfacial area but with fewer crystal layers and the resulting value of γ was found to be in agreement within error bars with that of the larger system, which indicated that no correction term was necessary.³ However, computation of γ for two different system sizes is computationally expensive since it involves implementation of all four stages of the cleaving wall method. We, therefore, explored the possibility that using EBAR method, we may be able to compute free energy accurately without the need to immobilize particles in the crystal layers.

We performed the computation for (111) orientation of the silicon crystal phase, since for this orientation the layers on the opposite sides of the cleaving plane are not symmetric. As a result, when the CM of the crystal phase fluctuates, it results in fluctuation of the cleaving potential, thus leading to hysteresis. For (100) orientation, this problem does not

occur because of the symmetry of layers on the opposite sides of the cleaving plane. As in Ref. 8, we employed crystal phase with 3024 particles and a simulation box with dimensions of $L_x = 3\sqrt{2}a$, $L_y = 3\sqrt{1.5}a$, and $L_z = 14\sqrt{3}a$, where $a = (8/\rho_C)^{1/3}$ is the unit cell length of the crystal phase and $\rho_C = 0.452\sigma^{-3}$ is the crystal density. The crystal phase contained 84 layers of (111) orientation in the z-direction, with 36 particles in each layer. The total configurational energy at a given value of z is given by

$$\phi(\mathbf{r}^N; z) = U(\mathbf{r}^N) + U_{ext}(\mathbf{r}^N; z), \quad (4)$$

where $\mathbf{r}^N = (\mathbf{r}_1, \dots, \mathbf{r}_N)$ is the instantaneous configuration of the particles, U_{ext} is the cleaving potential exerted by the wall, and z is the distance between the wall and the cleaving plane. The cleaving potential consisted of a repulsive two-body term and a 3-body term derived from Stillinger and Weber potential as explained in Ref. 8. The cleaving wall was constructed of two ideal crystal layers of (111) orientation with 36 particles in each layer.⁸ The cleaving planes were located at two boundaries of the simulation box in z-direction. The Helmholtz free energy change for cleaving of the crystal phase is given by the following expression:³

$$\begin{aligned} \Delta F &= \int_{z_i}^{z_f} dz \frac{\partial F}{\partial z} \\ &= \int_{z_i}^{z_f} dz \left\langle \frac{\partial \phi}{\partial z} \right\rangle, \end{aligned} \quad (5)$$

where $\langle \dots \rangle$ is canonical ensemble average at a particular value of z . Following Ref. 8, we chose the initial and final positions of the cleaving walls as $z_i = 1.80$ and $z_f = 0.75$, respectively. We performed canonical ensemble Monte Carlo (MC) simulations at various values of z with 50000 MC steps for equilibration and 2×10^5 steps for production run. Each MC step consisted of 3024 trial displacement moves. The maximum value of the attempted displacement during the trial moves was adjusted during the equilibration period to have an acceptance ratio of nearly 50 %. The integrand in Eq. (5) and the perturbation energy $[(\phi_1 - \phi_0)$ or $(\phi_0 - \phi_1)$ required in Eq. (1)] was sampled after every MC step.

Figure 1 shows the negative of the integrand in Eq. (5) per unit area (obtained without applying any constraint) as a function of the distance z . The results and the corresponding error bars reported in Fig. 1 and elsewhere represent the mean and the standard error of the estimates obtained from block averages during the production run. The ordinate in the plot is the magnitude of the force between the wall and the particles, which increases with

decreasing z because of the repulsive nature of the wall. The integrand shows large hysteresis throughout the path in the absence of the any constraint. However, when we apply the fixed layer constraint the hysteresis disappears as seen in the inset of Fig. 1. When performing simulations with the constraint,³ particles in two central layers (layers numbering 42 and 43) in the z -direction were fixed, i.e., trial moves attempting to displace the particles in these layers were rejected with certainty during MC simulation. A qualitative comparison of the plots shown in Fig. 1 confirms that fluctuations in the CM leads to the hysteresis. Note that due to the effect of the constraint on the free energy, the values of the integrand in the inset of Fig. 1 are significantly different from those in the main plot. Due to this hysteresis, the BAR method is expected to fail and hence we have applied the EBAR method as explained below.

In order to compute the free energy difference, we consider state 0 as the crystal phase with a cleaving wall distances of $z=1.8$ which is equal to the cut-off distance of the external potential. Thus, in state 0 no external potential acts on the system. As we decrease the value of z , the influence of the external potential acting on the system increases. In Figs. 2 and 3, we report the relevant details of the EBAR and the BAR methods when using data from two simulations at $z = 0.75$ (state 1) and 1.8 (state 0). As seen in Fig. 2, the BAR result, which corresponds to the condition $\partial\sigma^2/\partial C = 0$ (or equivalently $\Sigma_0 = \Sigma_1$), is in the small sample regime,¹⁰ since $\Sigma_0 = \Sigma_1 \ll 1$. Also, from the slope of the curve at $C = C_B$ in Fig. 3, we find that $\partial\Delta F/\partial C = -1$ which again confirms that the BAR result is in the small sample regime.¹⁰ Thus the optimization scheme fails and the BAR method result is far off from the actual value, as seen in Fig. 3. In the EBAR method, we choose a value of C_E (see Fig. 2) such that the magnitude of $\partial\sigma^2/\partial C$ is maximum and $\Sigma_0 \geq 1$. The corresponding value of ΔF (see Fig. 3) compares well with the accurate result reported in Ref. 8 using the BAR method. At a large positive value of $C > 220$, the value of $\Delta F/A$ computed using the acceptance ratio formula Eq. (1) approaches 0.0175 J/m^2 , which corresponds to the FEP formula in state 1. Thus, the EBAR method (see Fig. 3), yields more accurate results compared to single stage FEP method. This is expected since the EBAR method utilizes data from both the ensembles unlike the FEP method which relies on data from ensemble 1 alone.

Figure 4 compares the computational effort required to obtain $\Delta F/A$ using different methodologies (see also Table I). When considering more than two simulations ($N_s > 2$),

the EBAR method is applicable only to the last interval and hence is combined with the BAR method to obtain total free energy difference. As an example, when considering 4 simulations ($N_s = 4$) at $z = 0.75, 0.8, 0.85$, and 1.8 , the result reported under the combined method (C) (see Table 1 and Fig. 4) is a sum of BAR results from $z = 0.75$ to 0.85 and the EBAR result from $z = 0.85$ to 1.8 . Figure 4 shows that the EBAR method yields accurate value with just two simulations while the BAR method requires at least 9 simulations. It can also be seen that numerical integration using Gaussian Quadrature (GQ) technique using 3 simulations is close to the correct value, however the size of the error bar is still relatively large compared to the EBAR result. This clearly indicates that GQ will require 4 or more simulations to achieve the desired accuracy.

We also tested for the convergence of the EBAR method in Fig. 4 by using simulation data at intermediate z values. For example for $N_s = 2, 4$, and 6 , the EBAR method was applied to the intervals from $z = 0.75$ to 1.8 , $z = 0.85$ to 1.8 , and $z = 1.0$ to 1.8 , respectively. As the width of the interval reduces, the extent of the overlap between the configurations in state 1 and state 0 will increase. However, the CM becomes less localized in state 1 due to reduced strength of the external potential at higher value of z and hence the estimation of \sum_1 becomes less accurate for a given n_1 as discussed in Sec. II. Note also that the size of the error bars in Fig. 1 is larger for $z > 0.75$ compared to that for $z = 0.75$, indicating a larger hysteresis due to CM fluctuations. Since the accuracy of the EBAR method depends on \sum_1 , we find that it becomes less accurate (although marginally) for smaller intervals (see EBAR/Combined results in Table I and Fig. 4).

B. Constrained fluid λ -integration

Grochola⁶ introduced constrained fluid λ -integration method to compute the free energy difference between the crystal and the melt phases. A major advantage of this method compared to traditional TDI methods¹ is that it *directly* calculates the free energy difference between the melt and the crystal phases by constructing a reversible path between the two phases. Thus, there is no need to connect the crystal and the melt phases *separately* to reference phases of known free energy and this gives more flexibility in terms of designing the reversible path. Grochola's method has been applied to calculate melting temperature of complex potentials for Sodium Chloride,¹⁸ Benzene and trizole.¹⁹ Further, the method

was extended to isothermal isobaric ensemble,⁷ and to computation of melting temperature of binary mixtures²⁰ and interfacial free energy of crystal phases.⁴

Here we compute Gibbs free energy difference between crystal and melt phases of silicon by *NPT* version⁷ of the constrained fluid λ - integration method. The expressions for the potential energy for the 3 stages of the reversible path are as given below:

$$\phi_1(\lambda_1) = (1 - \eta\lambda_1)U, \quad (6)$$

$$\phi_2(\lambda_2) = (1 - \eta)U + \lambda_2 U_{ext}, \quad (7)$$

and

$$\phi_3(\lambda_3) = [(1 - \eta) + \lambda_3\eta]U + (1 - \lambda_3)U_{ext}, \quad (8)$$

where U is the potential energy due to interactions between the system particles, η is a parameter controlling the extent to which strength of interaction is reduced in the first stage.^{6,7} λ_1 , λ_2 , and λ_3 are the parameters characterizing the three stages. The Gaussian external potential imposed during the second and the third stage is given by^{6,7} $U_{ext} = \sum_i \sum_k a \exp(-br_{ik}^2)$, where the summation with respect to i is taken over all the particles, r_{ik} is the distance between the i th particle and k th well, and the summation with respect to k is taken over all Gaussian potential wells within a certain cutoff distance of the i th particle. A constraint on the maximum possible volume V_m along the path is imposed⁷ to ensure thermodynamic reversibility. The Gibbs free energy change for the third stage of the path is given by:⁷

$$\Delta G_3 = \int_0^1 d\lambda_3 \langle \eta U - U_{ext} \rangle, \quad (9)$$

where $\langle \dots \rangle$ represents the isothermal–isobaric ensemble average at a given value of λ_3 . Similar expressions apply for ΔG_1 and ΔG_2 .⁷

The simulation at a given state point along the path was performed in *NPT* ensemble with $N = 1000$ particles confined to a cubic simulation box under periodic boundary conditions. At a given state point, we used 15000 MC steps for equilibration and 20000 steps for production, except at the end of 3rd stage, where 10^5 MC steps were used for production run from $\lambda_3 = 0.94$ to 1. In each MC step, we attempted, on average, two volume change moves and 1000 particle displacement moves. The size of the attempted changes was adjusted during equilibration steps so as to achieve an acceptance ratio of about 50%. During production run, we sampled the integrand for TDI method and the perturbation

energy for BAR method after every MC step. The Gaussian well parameters were chosen to be $a = -1.892\epsilon$ and $b = 8.0\sigma$ in accordance with the criteria mentioned in Refs. 7,20. The parameter η in Eqs. (6)–(8) was assigned a value of 0.9 following earlier work.^{6,7} Further, we chose the maximum volume to be $V_m^* = N/0.4$ at $T^* = 0.0667$ and $P^* = 0$ so that V_m does not affect the free energy of the crystal or the melt phases.⁷

We found no hysteresis for the first two stages of the path as in earlier studies.⁶ In the third stage, however, we found hysteresis between $\lambda_3 = 0.99$ to 1.0 as seen in the inset of Fig. 5. The reason for this hysteresis is that as ($\lambda_3 \rightarrow 1$), the influence of the external potential on the crystal phase becomes negligible as can be seen in expression of ϕ_3 in Eq. (8), which results in fluctuations of the CM position. Note that in computations performed by Grochola (see Fig. 6 of Ref. 6), no hysteresis was seen in the third stage, because zero CM velocity was maintained during MD simulations. In order to compute the free energy difference in stage 3, we denote state corresponding to $\lambda_3 = 1$ as state 1, in which no external potential acts on the crystal phase. Note that the role of states 0 and 1 is reversed compared what we discussed earlier since the external potential is acting in state 0 ($\lambda_3 < 1$) in the present case. As λ_3 is decreased, the influence of the external potential increases. We compared BAR, EBAR, GQ methods on the basis of number of simulations (N_s) performed at various values of λ_3 between 0.9 and 1 to obtain a given result. For $N_s > 2$, the EBAR result is applicable only to the last interval and hence we combine it with the BAR result for the rest of the intervals as explained before. (Also note that Eq. (1) will yield ΔG instead of ΔF since we are dealing with NPT ensemble as mentioned at the end of sec. II).

Figure 6 and 7 show the results for the BAR and the EBAR results using two simulations performed at $\lambda_3 = 0.94$ (state 0) and 1 (state 1). As seen in Fig. 6, the BAR result is in the small sample regime since $\Sigma_0 = \Sigma_1 \ll 1$. Also, we find that $\partial\Delta G/\partial C = -1$ at $C = C_B$ from the slope of the plot in Fig. 7, which again indicates a small sample regime.¹⁰ As a result, the BAR result shows a large deviation from the actual value as seen in Fig. 7. On the other hand, the EBAR result (which corresponds to the maxima of $|\partial\sigma^2/\partial C|$ such that $\Sigma_1 \geq 1$) is quite accurate as seen in Figs. 6 and 7. Note that as C approaches a large negative value $C < -1170$, the ΔG value approaches $-33.8 k_B T$ which corresponds to the FEP formula in state 0. Thus, the EBAR method yields more accurate results compared to both the single stage FEP method and the BAR method.

In Fig. 8, we have tested the convergence of the results in the interval from $\lambda_3 = 0.9$ to 1.

(Note that the figure shows the total Gibbs free energy difference ΔG_T for the entire path and all the results reported in the figure include a contribution of $60.75 \pm 3 k_B T$ from $\lambda_1 = 0$ to $\lambda_3 = 0.9$ computed by BAR method). As can be seen in the figure, BAR method requires 12 simulations to obtain acceptable accuracy. On the other hand, EBAR (combined) method yields sufficiently accurate value of ΔG_T with 4 simulations. Using the converged result in Fig. 8, we find that the contribution of the CM hysteresis to the total error in ΔG_T is about $\pm 2 k_B T$. We also found the thermodynamic integration using Gaussian Quadrature (GQ) method yields sufficiently accurate result with just 2 simulations in comparison to 4 simulations required by the EBAR method. In this case, GQ technique is effective because the integrand changes smoothly (although rapidly) as λ_3 approaches 1 and moreover GQ does not require evaluation of the integrand at $\lambda_3 = 1$ which is most prone to hysteresis.

As for the convergence of the EBAR method, we note that for $N_s = 2$ (see Table I and Fig. 8), the EBAR result (applied in the interval from $\lambda_3 = 0.9$ to 1) deviates significantly from the accurate value. This is because the external potential starts affecting the structure of the crystal phase significantly [see Eq. (8)] for $\lambda_3 \leq 0.9$ (state 0) and hence the value of Σ_0 becomes less accurate, as discussed in Sec. II. As we increase N_s , the EBAR (combined) result converges rapidly as seen in Fig. 8. This is because even for $\lambda_3 = 0.99$ the CM position is sufficiently localized and hence Σ_0 evaluation is accurate. This can also be seen in the inset of Fig. 5, which shows that the CM hysteresis becomes appreciable only for $\lambda_3 > 0.995$.

Finally, based on the value of ΔG_T , we also computed the melting temperature (T_m) by integrating the following equation at $P^* = 0$:⁵

$$k_B T^2 \left[\frac{\partial(\Delta G_T/k_B T)}{\partial T} \right]_{P,N} = (\langle U \rangle_L + P \langle V \rangle_L) - (\langle U \rangle_S + P \langle V \rangle_S), \quad (10)$$

where $\langle \dots \rangle_L$ and $\langle \dots \rangle_S$ denote the NPT ensemble averages for the liquid and crystal phases at the specified temperature. We found the value of T_m to be 1675 ± 5 K, based on EBAR (combined) result with $N_s = 4$. This is in close agreement with the value of 1678 K obtained in Ref. 14 by crystal-melt coexistence simulations for Si(100) interface and the value of 1691 ± 20 K obtained in Ref. 21.

IV. SUMMARY

In this work, we have shown that EBAR method efficiently calculates the free energy of the crystal phase due to an external potential without requiring use of a constraint on the translational degrees of freedom. In this method, we nullify the error incurred due to poor sampling of the perturbation energy in state 0 (crystal phase without the external potential) by adjusting the value of the shift constant C [see Eq. (1)] so that the error in estimated free energy difference is completely due to state 1 (the state in which an external potential acts on the crystal phase), where we expect the sampling of the perturbation energy to be sufficiently accurate. We have applied this technique to cleaving wall method, in which the crystal phase is subjected to a repulsive cleaving potential³ and confined fluid λ -integration method,⁶ in which the crystal phase is acted upon by attractive Gaussian potential wells located at the ideal crystal lattice sites. In both cases, we found that EBAR method yields accurate values with reasonable computational effort and offers considerably improvement over both the single stage FEP method (in state 1) and the BAR method. Note that unlike the FEP method, the EBAR method utilizes information from both the ensembles.

It must be stressed that the EBAR method is applicable only when the BAR result is in the small sample regime. Thus, the domains of applicability of the two methods are mutually exclusive. With regard to the convergence, we found that the EBAR method ceases to be accurate in the following limits: (i) When the external potential is too weak so that the CM position is not localized as seen in cleaving wall method (see Fig. 4 and Table I) and (ii) when the external potential is too strong so as to affect the crystal structure significantly as in the case of constrained fluid λ -integration method (see Fig. 8 and Table I). Both of these conditions increase the error the computation of \sum_1 (corresponding to the state in which external potential is acting). The EBAR method is simple to implement since it only requires that the perturbation energies in the two states be sampled and does not depend upon the existence of a reversible path connecting the two states.

In the constrained fluid λ -integration method, thermodynamic integration by GQ technique is found to be effective since the CM hysteresis is confined to the end of the integration path (see Fig. 5). However, the GQ technique suffers from the inherent drawback of the TDI method in that it depends upon the existence of a reversible path between the two thermodynamic states. Also, testing the convergence of this technique is relatively expen-

sive since the abscissa values for higher number of integration points do not coincide with those corresponding to lower number of integration points.²² These problems prevent general applicability of the GQ technique, as in the case of the cleaving wall method where the CM hysteresis occurs throughout the path (see Fig. 1).

We expect that EBAR method will also be useful in computing bulk crystal phase free energy by Einstein crystal method¹ and in computing surface free energy of crystal phases⁴ where the CM hysteresis occurs. It seems possible to generalize the EBAR method to other free energy computations. Our initial calculations indicate that the EBAR method can also be applied to the cleaving of the crystal-melt interface (state 4 of the cleaving wall method), which is considered as a major challenge in the computation of the crystal-melt interfacial energy.^{3,12} Here the crystal-melt interface fluctuates in the absence of the external potential while it is held fixed when external cleaving potential is present.³ It will be interesting to explore the applicability of EBAR method to the computation of the chemical potential by particle insertion-deletion technique.¹ Here the perturbation energies due to the particle insertion steps are sufficiently accurate while those due to the particle deletion steps are not sampled efficiently. This situation is similar to the problem considered in this article.

Acknowledgments

The author would like to thank Professors X. C. Zeng and I. Kusaka for helpful discussions. This work was supported by the research initiation grant provided by the Indian Institute of Technology, Kanpur.

¹ D. Frenkel and B. Smit, *Understanding Molecular Simulation* (Academic Press, San Diego, 2002), 2nd ed.

² J. R. Fernandez and P. Harrowell, *J. Chem. Phys.* **120**, 9222 (2004).

³ R. L. Davidchack and B. B. Laird, *J. Chem. Phys.* **118**, 7651 (2003).

⁴ G. Grochola, I. K. Snook, and S. P. Russo, *J. Chem. Phys.* **122**, 064711 (2005).

⁵ J. Q. Broughton and G. H. Gilmer, *J. Chem. Phys.* **79**, 5095 (1983).

⁶ G. Grochola, *J. Chem. Phys.* **120**, 2122 (2004).

⁷ P. A. Apte and I. Kusaka, *Phys. Rev. E* **73**, 016704 (2006).

- ⁸ P. A. Apte and X. C. Zeng, Appl. Phys. Lett. **92**, 221903 (2008).
- ⁹ F. H. Stillinger and T. A. Weber, Phys. Rev. B **31**, 5262 (1985).
- ¹⁰ C. H. Bennett, J. Comput. Phys. **22**, 245 (1976).
- ¹¹ M. R. Shirts and V. S. Pande, J. Chem. Phys. **122**, 144107 (2005).
- ¹² Y. Mu and X. Song, J. Chem. Phys. **124**, 034712 (2006).
- ¹³ N. Lu, J. K. Singh, and D. A. Kofke, J. Chem. Phys. **118**, 2977 (2003).
- ¹⁴ S. Yoo, X. C. Zeng, and J. R. Morris, J. Chem. Phys. **120**, 1654 (2004).
- ¹⁵ R. L. Davidchack and B. B. Laird, Phys. Rev. Lett. **85**, 4751 (2000).
- ¹⁶ R. L. Davidchack and B. B. Laird, J. Phys. Chem. B **109**, 17802 (2005).
- ¹⁷ R. Handel, R. L. Davidchack, J. Anwar, and A. Brukhno, Phys. Rev. Lett. **100**, 036104 (2008).
- ¹⁸ D. M. Eike, J. F. Brennecke, and E. J. Maginn, J. Chem. Phys. **122**, 014115 (2005).
- ¹⁹ D. M. Eike and E. J. Maginn, J. Chem. Phys. **124**, 154504 (2006).
- ²⁰ P. A. Apte and I. Kusaka, J. Chem. Phys. **123**, 194503 (2005).
- ²¹ J. Q. Broughton and X. P. Li, Phys. Rev. B **35**, 9120 (1987).
- ²² W. H. Press, S. A. Teukolsky, W. T. Vetterling, and B. P. Flannery, *Numerical Recipes* (Cambridge University Press, Cambridge, 1992).

TABLE I: The number of simulations (N_s) and the free energy calculations obtained by the BAR (B), EBAR (E) and the combined (C) results. In the combined results ($N_s > 2$), the EBAR method is applied for the last interval while the BAR method is applied for the rest of the intervals. The second and the third column relate to the cleaving wall method, while the last two columns relate to the constrained fluid λ -integration method. The data contained in this table is also plotted in Figs. 4 and 8.

N_s	z values	$\Delta F/A$ (J/m ²)	λ values	$\Delta G_T/k_B T$
2	0.75, 1.80	0.041 ± 0.002 (E) 0.36 ± 0.15 (B)	0.9, 1.0	28.6 ± 7.1 (E)
4	0.75, 0.80, 0.85 1.80	0.0455 ± 0.005 (C)	0.9, 0.92, 0.94 1.0	12.4 ± 4.6 (C) -576 ± 193 (B)
6	0.75, 0.80, 0.85 0.90, 1.00, 1.80	0.0054 ± 0.009 (C) 0.088 ± 0.024 (B)	0.9, 0.92, 0.94 0.95, 0.96, 1.0	9.0 ± 4.4 (C) -379 ± 130 (B)
9	0.75, 0.80, 0.85 0.90, 1.00, 1.10 1.20, 1.50, 1.80	0.0439 ± 0.004 (B)	0.9, 0.92, 0.94 0.95, 0.96, 0.97 0.98, 0.99, 1.0	5.5 ± 4.4 (C) -87.9 ± 34.4 (B)

FIG. 1: The variation of the integrand in Eq. (5) as a function of z at $T^* = 0.0667$, and $\rho_C = 0.452\sigma^{-3}$ for cleaving of Si(111) crystal phase. The inset shows the same plot with a fixed layer constraint. In applying this constraint the particles in the middle layers (layers numbering 42 and 43) were immobilized. Note that due to the effect of the constraint on the free energy, the value of integrand at a given z is significantly larger in the inset plot. The error bars are seen when these are larger than the size of the symbols.

FIG. 2: The criteria for choosing values of C for the BAR and the EBAR methods. The data is generated from simulations done at $z = 1.8$ (state 0 with the external potential) and $z = 0.75$ (state 1 without the external potential). The BAR result corresponds to the condition that $\sum_0 = \sum_1$ while the EBAR result corresponds to the maximum of $|\partial\sigma^2/\partial C|$ such that \sum_0 is of order unity or higher. A local maximum also exists when $\sum_1 \geq 1$, but is not seen in the figure because of its small magnitude.

FIG. 3: The value of Free energy difference per unit area (in units of J/m^2) obtained by Eq. (1) for the same set of data as that in Fig. 2. The inset shows more detailed comparison of the EBAR result with that of Ref. 8 (dashed line). From the slope of the plot, we get $\partial\Delta F/\partial C = -1$ at $C = C_B$ indicating a small sample regime for the BAR result.¹⁰ At the two end points of the graph ($C = -10$ and $C = 220$), the value of ΔF approach those obtained from the FEP formulas in the two ensembles.

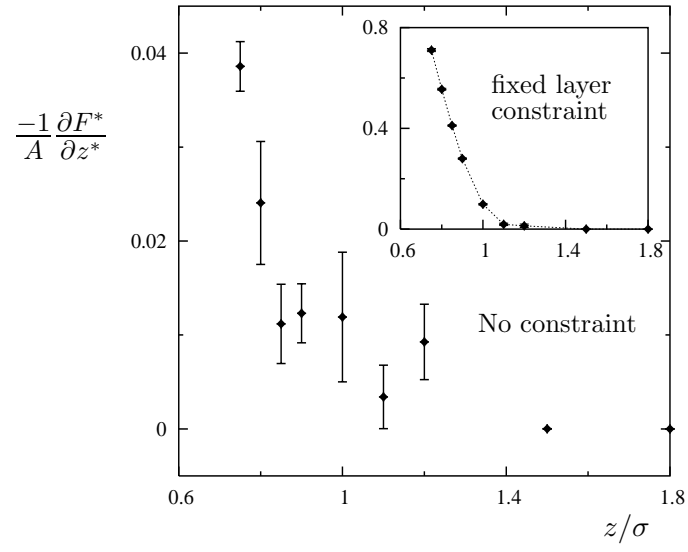
FIG. 4: Free energy change per unit area (in J/m^2) resulting for cleaving of Si(111) crystal phase without any constraint. The error bars are seen when these are larger than the size of the symbols. The abscissa represents the number of simulations (N_s) performed at different values of z (see Table I). The horizontal line represents the result obtained using the BAR method in Ref. 8. The combined result (applicable for $N_s > 2$), represents a combination of the EBAR and the BAR methods as explained in the text.

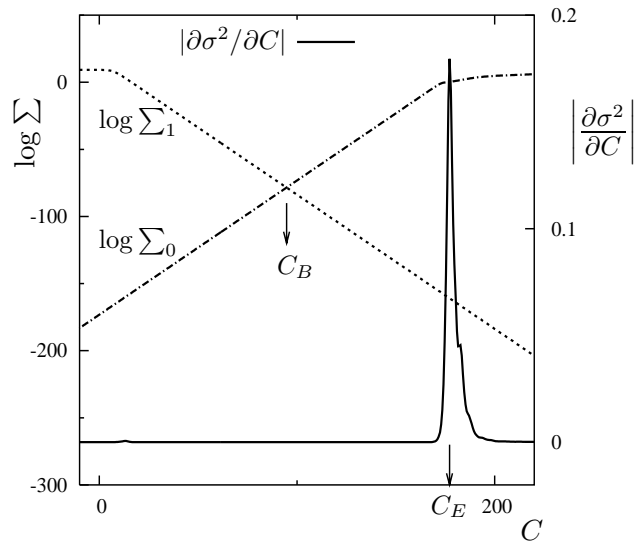
FIG. 5: The variation of the integrand in Eq. (9) as a function of λ_3 at $P^* = 0.0$, $T^* = 0.0667$, and $N = 1000$ for the forward and the backward runs for stage 3. The inset shows the region of maximum hysteresis.

FIG. 6: The criteria for choosing appropriate values of C for the BAR and the EBAR methods. The data is generated from simulations performed at $\lambda_3 = 0.94$ (state 0) and $\lambda_3 = 1.0$ (state 1). The external Gaussian potential acts in state 0 while it is absent in state 1 according to Eq. (8). The values of the Gibbs free energy difference ΔG between the two ensembles are plotted as a function of C in Fig. 7. The BAR result corresponds to the condition that $\sum_0 = \sum_1$ while the EBAR result corresponds to the maximum of $|\partial\sigma^2/\partial C|$ such that $\sum_1 \geq 1$.

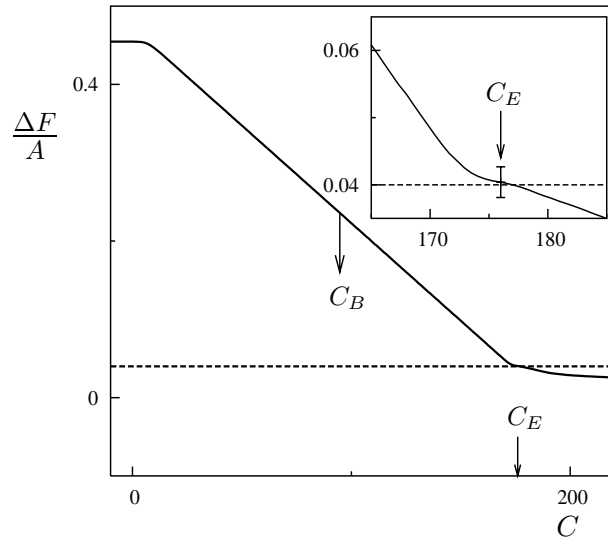
FIG. 7: The value of Gibbs free energy difference (in units of $k_B T$) between $\lambda_3 = 0.94$ and 1.0 states. The result is obtained by Eq. (1) for the same set of data as that in Fig. 6. Note that the slope of the curve is -1 at $C = C_B$ indicating a small sample regime for the BAR result. The inset shows more detailed comparison of the EBAR result with the accurate result (dashed line) obtained by inserting several intermediate steps between $\lambda_3 = 0.94$ and 1. At the two ends of the plot ($C = -1170$ and $C = 0$) ΔG values approach those corresponding to the FEP formulas in the two ensembles.

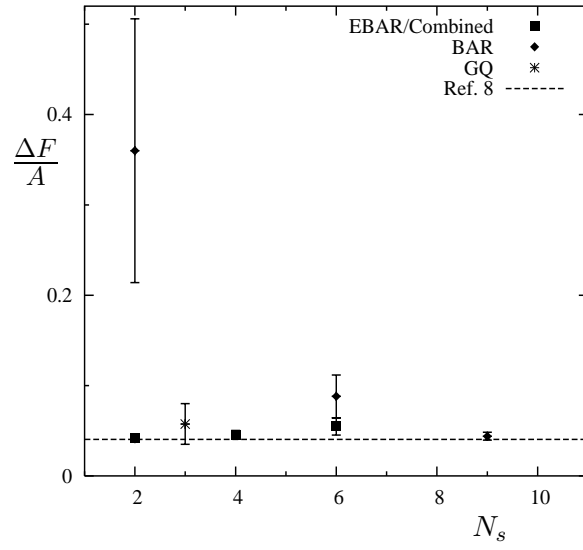
FIG. 8: Total Gibbs Free energy difference (in units of $k_B T$) between the melt and the crystal phases obtained without applying any constraint. All of the results include a contribution of $60.75 \pm 3 k_B T$ from $\lambda_1 = 0$ to $\lambda_3 = 0.9$ as mentioned in the text. The abscissa represents the number of simulations performed at various values of λ_3 between 0.9 and 1. The horizontal line represents the converged value obtained by the BAR method with $N_s = 12$ (see the inset). The size of the error bar for this converged result is of the same magnitude as the combined result with $N_s = 9$.

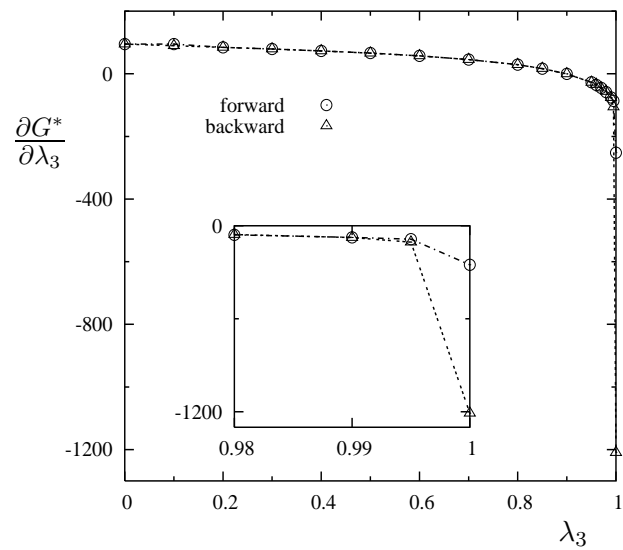


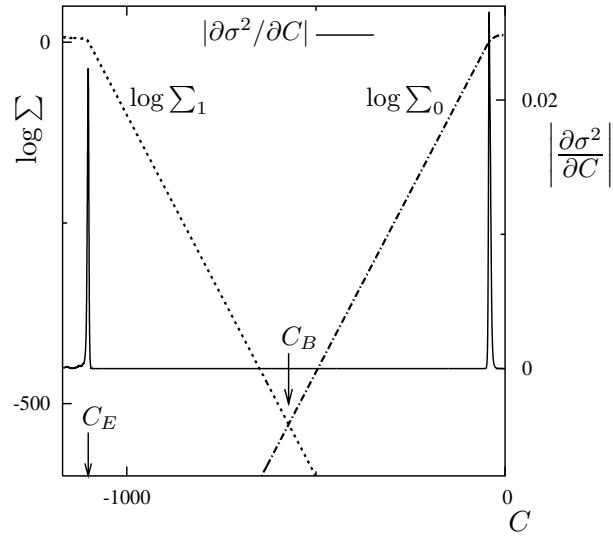


P. A. Apte, FIG. 2









P. A. Apte, FIG. 6

